Journal of Computational Mathematics
Vol.35, No.1, 2017, 37–51.

http://www.global-sci.org/jcm
doi:10.4208/jcm.1607-m2014-0109

ENERGY STABLE NUMERICAL METHOD FOR THE TDGL EQUATION WITH THE RETICULAR FREE ENERGY IN HYDROGEL*

Dong Liao
School of Mathematics and Statistics, Nanyang Normal Univeristy, Nanyang 473061, China
Email: 7775024@163.com
Hui Zhang and Zhengru Zhang
Laboratory of Mathematics and Complex Systems, Ministry of Education
and School of Mathematical Sciences, Beijing Normal University, Beijing 100875, China
Email: hzhang@bnu.edu.cn, zrzhang@bnu.edu.cn

Abstract

Here we focus on the numerical simulation of the phase separation about macromolecule microsphere composite (MMC) hydrogel. The model is based on time-dependent Ginzburg-Landau (TDGL) equation with the reticular free energy. An unconditionally energy stable difference scheme is proposed based on the convex splitting of the corresponding energy functional. In the numerical experiments, we observe that simulating the whole process of the phase separation requires a considerably long time. We also notice that the total free energy changes significantly in initial stage and varies slightly in the following time. Based on these properties, we apply the adaptive time stepping strategy to improve the computational efficiency. It is found that the application of time step adaptivity can not only resolve the dynamical changes of the solution accurately but also significantly save CPU time for the long time simulation.

Mathematics subject classification: 65M06, 65M12, 65Z05.
Key words: TDGL equation, Unconditionally energy stable scheme, Adaptive time-stepping method, Phase transition.

1. Introduction

Hydrogels, which are polymer with 3-D crosslinked hydrophilic network structure, have increasingly extensive applications in industrial and biomedical fields [9,10,26]. Therefore, hydrogels have recently received tremendous attention in scientific communities due to their enhanced properties [1, 16]. Comparing with traditional hydrogels with poor mechanism, recently there has been a lot of novel methods to improve the structure of hydrogels and thus significantly enhancing their mechanical properties [9,10,12], e.g., topological (TP) gels [3,4], nanocomposite (NC) hydrogels [8], double-network (DN) gels [4, 7], MMC hydrogels and so on [9, 10]. MMC hydrogels, which were synthesized by Ting Huang in 2007 [9], have a unique well-defined microstructure and very high mechanical strength. MMC hydrogels are environmentally sensitive and mainly possible to use in drug delivery and other biomedical applications [22]. Many works in chemical structure and dynamics simulation have been done about TP gels, NC hydrogels, and DN gels and much progress has been made [5,11,12,25]. But there are relatively less results about MMC hydrogels [23,24]. Why the MMC hydrogels have such high mechanical strengths?

* Received October 24, 2014 / Revised version received June 13, 2016 / Accepted July 5, 2016 / Published online January 18, 2017 /

What are relation between the structure and property? The structural factors: nanoparticle size, grafting density, polymer chain length, chain conformation, entanglement, how to influent the phase transition? These problems are very important. Now we have investigated the microscopic structures in [24] and large deformation of the MMC hydrogels in [23]. The MMC-TDGL model have been given to get the phase transition of the MMC hydrogels [26]. But it is very large for the computational cost of the MMC-TDGL model. In the following we will introduce the model in details.

Meanwhile, many computational methods have been developed and applied in modeling and simulation of phase separation of hydrogels. They range from molecular scale (e.g., molecular dynamics, Monte Carlo), microscale (e.g., Brownian dynamics, dissipative particle dynamics, lattice Boltzmann, TDGL method, dynamic density functional theory method) to mesoscale and macroscale (e.g., micromechanics, equivalent-continuum and self-similar approaches, finite element method) [25]. These methods are foundation to simulate phase separation of hydrogels. However, observing the whole process of phase separation is computationally expensive and costs a large amount of time when these methods are used. Therefore, seeking for algorithms to decrease computation cost is an urgent task. The adaptive time-stepping method is introduced here. Adaptive time stepping method has been well studied for solving initial value problems in ODEs. The review work [18, 19] summarizes several step control methods for local time adaptivity based on linear feedback theory. A locally varying time step method is developed for solving hyperbolic conservative PDEs where large time step is adopted on region with smooth solution while small time step is taken in domain with nearly singular solution within same time level [20]. In [17], the adaptive time-stepping technique has been developed based on energy variation which is an important physical quantity in the molecular beam epitaxy growth model. Following [17], we improve the choice of adaptive time step according to properties of TDGL equation.

In this work, considering the MMC hydrogels have microstructure with network crosslinking points, we exploit the TDGL method to simulate phase evolution of MMC hydrogels based on reticular free energy deduced in [26], called as the MMC-TDGL model. TDGL method is an accurate and robust method to simulate structural evolution of phase separation in polymer blends and copolymers and many nice results have been gotten in numerical experiments [1, 14, 25]. The main objective of this work is to develop an unconditional energy stable method for the MMC-TDGL model and apply adaptive time step strategy to the algorithm. Our numerical approach is based on the convex splitting of the discrete energy functional. The convex part is discretized using implicit scheme, while the concave part is handled by using explicit scheme. The mass conservation and energy law in discrete sense are proved theoretically. The unique solvability is obtained by minimizing an equivalent convex discrete functional. A couple of numerical experiments are implemented to observe the phase evolution of the model. And also the effectiveness of the adaptive time step method is shown clearly by comparing the CPU time. During the time period with rapid free energy decay, small adaptive time steps are chosen adaptively, while large time steps are used when free energy varies slowly.

This paper is organized as follows. In Section 2, the MMC-TDGL equation is introduced in detail with the reticular free energy. The model is derived based on the variational derivative of the corresponding energy functional. In Section 3, the unconditional energy stable scheme is proposed and some numerical analysis are given. In Section 5, some numerical experiments are performed to observe the phase evolution of the model. In Section 6, based on observations, we propose a suitable adaptive time-stepping strategy and show the effectiveness numerically.

Some concluding remarks are made in the final section.

2. MMC-TDGL Equation

TDGL equation is a microscale method for simulating the structural evolution of phase-separation in polymer blends and block copolymers. Here we consider a dimensionless energy of the model, total Flory-Huggins-de Gennes free energy E can be defined as:

$$E[\phi(\mathbf{x},t)] = \int_\Omega [F(\phi(\mathbf{x},t)) + k_B T\kappa|\nabla\phi(\mathbf{x},t)|^2]d\mathbf{x}, \tag{2.1}$$

where κ is a constant, k_B is Boltzmann constant and T is temperature constant [2]. $\phi(\mathbf{x},t)$ is order parameter, by definition $\phi \in (0,1)$. It is pointed out that for a binary polymer blend, $F(\phi(\mathbf{x},t))$ usually denotes the Flory-Huggins free energy. However, as mentioned before, MMC hydrogels have network structure. Hence, in [26], it is proved that the reticular free energy should be defined as follows.

$$F = k_B T\left(\frac{\phi}{\tau}\ln(\frac{\alpha\phi}{\tau}) + \frac{\phi}{N}\ln(\frac{\beta\phi}{\tau}) + (1-\rho\phi)\ln(1-\rho\phi) + \chi\rho\phi(1-\rho\phi)\right), \tag{2.2}$$

where the parameters τ, α, β, N, and ρ are constants [26]. χ is the enthalpic interaction parameter between two polymer components. As derived in [26], it can be guaranteed that $(1-\rho\phi) > 0$. The MMC-TDGL model can be written as follows [1, 14, 25, 26].

$$\frac{\partial\phi(\mathbf{x},t)}{\partial t} = \nabla\cdot(M(\phi)\nabla\mu), \tag{2.3}$$

where the mobility M may depend on ϕ, μ is the chemical potential defined as

$$\mu := \delta_\phi E = F'(\phi) - 2k_B T\kappa\Delta\phi$$

with

$$F'(\phi) = k_B T\left(\frac{1}{\tau}\ln(\frac{\alpha\phi}{\tau}) + \frac{1}{\tau} + \frac{1}{N}\ln(\frac{\beta\phi}{\tau}) + \frac{1}{N} - \rho\ln(1-\rho\phi) - \rho + \chi\rho - 2\chi\rho^2\phi\right).$$

Below we consider the case of constant M.

Combining the above equations, we get the following model

$$\frac{\partial\phi}{\partial t} = \nabla\cdot(\nabla M F'(\phi)) - 2Mk_B T\kappa\Delta^2\phi. \tag{2.4}$$

Multiplying (2.3) by μ and integrating over Ω, we get

$$\frac{dE}{dt} = \int_\Omega \mu\phi_t d\mathbf{x} = \int_\Omega \mu\nabla\cdot(M\nabla\mu)\, d\mathbf{x}.$$

The above equality holds because of the fact that E is independent of variable $\mathbf{x}$ according to definition of E in (2.1). Then, considering periodic boundary condition for ϕ and by divergence theorem, we easily get

$$\frac{dE}{dt} = -\int_\Omega M|\nabla\mu|^2 d\mathbf{x} \le 0. \tag{2.5}$$

Therefore, we know that the total free energy of the whole system is decreasing over time.

3. Unconditionally Energy Stable Scheme

We first discuss the properties of the energy functional (2.1) which will be divided into two parts (refer to [6, 21]). Then we will present the semi-discrete scheme for the MMC-TDGL model (2.1) and prove some properties theoretically.

Lemma 3.1. *Suppose the solution ϕ of the equation* (2.4) *is periodic and sufficiently regular. Define*

$$E_c(\phi) = \int_\Omega k_B T[\frac{\phi}{\tau}\ln(\frac{\alpha\phi}{\tau}) + \frac{\phi}{N}\ln(\frac{\beta\phi}{\tau}) + (1-\rho\phi)\ln(1-\rho\phi) + \kappa|\nabla\phi|^2]d\mathbf{x}; \quad (3.1)$$

$$E_e(\phi) = \int_\Omega -k_B T\chi\rho\phi(1-\rho\phi)d\mathbf{x}\,. \quad (3.2)$$

Then $E_c(\phi)$ and $E_e(\phi)$ are both convex with respect to ϕ.

Proof. Let

$$e_c(\phi,\phi_x,\phi_y) = k_B T(\frac{\phi}{\tau}\ln(\frac{\alpha\phi}{\tau}) + \frac{\phi}{N}\ln(\frac{\beta\phi}{N}) + (1-\rho\phi)\ln(1-\rho\phi) + \kappa|\nabla\phi|^2), \quad (3.3)$$

$$e_e(\phi,\phi_x,\phi_y) = -k_B T\chi\rho\phi(1-\rho\phi). \quad (3.4)$$

Then

$$E_c(\phi) = \int_\Omega e_c(\phi,\phi_x,\phi_y)d\mathbf{x}, \quad E_e(\phi) = \int_\Omega e_e(\phi,\phi_x,\phi_y)d\mathbf{x}\,.$$

It is easy to get

$$\begin{aligned}
&\partial^2_\phi e_c(\phi,\phi_x,\phi_y) = k_B T\left(\frac{1}{\tau\phi} + \frac{1}{N\phi} + \frac{\rho^2}{1-\rho\phi}\right) > 0,\\
&\partial^2_{\phi_x} e_c(\phi,\phi_x,\phi_y) = 2k_B T\kappa \geq 0,\\
&\partial^2_{\phi_y} e_c(\phi,\phi_x,\phi_y) = 2k_B T\kappa \geq 0,\\
&\partial^2_\phi e_e(\phi,\phi_x,\phi_y) = 2k_B T\chi\rho^2 \geq 0.
\end{aligned}$$

This indicates that $e_c(\phi,\phi_x,\phi_y)$ and $e_e(\phi,\phi_x,\phi_y)$ are both convex in all of its arguments, thus we have the following inequality according to the definition of convex function:

$$e_c(\lambda\mathbf{u} + (1-\lambda)\mathbf{v}) \leq \lambda e_c(\mathbf{u}) + (1-\lambda)e_c(\mathbf{v}), \quad (3.5)$$

$$e_e(\lambda\mathbf{u} + (1-\lambda)\mathbf{v}) \leq \lambda e_e(\mathbf{u}) + (1-\lambda)e_e(\mathbf{v}), \quad (3.6)$$

where $\mathbf{u} = (\phi,\phi_x,\phi_y)^T$, $\mathbf{v} = (\psi,\psi_x,\psi_y)^T$. Integrating both sides of (3.5) and (3.6) leads to

$$\begin{aligned}
&E_c(\lambda\phi + (1-\lambda)\psi) \leq \lambda E_c(\phi) + (1-\lambda)E_c(\psi),\\
&E_e(\lambda\phi + (1-\lambda)\psi) \leq \lambda E_e(\phi) + (1-\lambda)E_e(\psi),
\end{aligned}$$

which proves that E_c and E_e are both convex. □

Lemma 3.2. *Suppose ϕ is the solution of the equation* (2.4) *with periodic boundary conditions and ϕ is sufficiently regular. Then it holds that*

$$E(\phi) - E(\psi) \leq (\delta_\phi E_c(\phi) - \delta_\phi E_e(\phi), \phi - \psi). \quad (3.7)$$

Proof. According to the previous lemma, we know that $e_c(\mathbf{u})$ is convex in all of its arguments ϕ, ϕ_x, ϕ_y, then

$$e_c(\mathbf{v}) - e_c(\mathbf{u}) \geq \nabla_{\mathbf{u}} e_c(\mathbf{u}) \cdot (\mathbf{v} - \mathbf{u}), \tag{3.8}$$

where $\mathbf{u} = (\phi, \phi_x, \phi_y)^T$ and $\mathbf{v} = (\psi, \psi_x, \psi_y)^T$. Integrating both sides of (3.8), we get

$$\begin{aligned} E_c(\psi) - E_c(\phi) &\geq \int_\Omega \left[\partial_\phi e_c(\mathbf{u})(\psi - \phi) + \partial_{\phi_x} e_c(\mathbf{u})(\psi_x - \phi_x) + \partial_{\phi_y} e_c(\mathbf{u})(\psi_y - \phi_y)\right] d\mathbf{x} \\ &= \int_\Omega \delta_\phi E_c(\phi)(\psi - \phi) d\mathbf{x} = (\delta_\phi E_c(\phi), \psi - \phi). \end{aligned} \tag{3.9}$$

Similarly, for $E_e(\phi)$ we also get

$$E_e(\psi) - E_e(\phi) \geq (\delta_\phi E_e(\phi), \psi - \phi). \tag{3.10}$$

Adding (3.9) and (3.10) yields

$$\begin{aligned} E(\psi) - E(\phi) &= (E_c(\psi) - E_e(\psi)) - (E_c(\phi) - E_e(\phi)) \\ &\geq (\delta_\phi E_c(\phi), \psi - \phi) + (\delta_\phi E_e(\psi), \phi - \psi) \\ &= (\delta_\phi E(\phi) - \delta_\phi E(\psi), \psi - \phi). \end{aligned}$$

This completes the proof of the lemma. □

Based on the convex splitting of the discrete energy, we now design the semi-discrete scheme for the MMC-TDGL model

$$\frac{\phi^{n+1} - \phi^n}{\Delta t} = M \Delta \mu^n, \tag{3.11}$$

where the numerical chemical potential is designed as

$$\begin{aligned} \mu^n &= \delta_\phi E_c(\phi^{n+1}) - \delta_\phi E_e(\phi^n) \\ &= k_B T \left(\frac{1}{\tau} \ln \frac{\alpha \phi^{n+1}}{\tau} + \frac{1}{N} \ln \frac{\beta \phi^{n+1}}{\tau} - \rho \ln(1 - \rho \phi^{n+1}) - 2\kappa \Delta_h \phi^{n+1} \right) - 2 k_B T \chi \rho^2 \phi^n. \end{aligned}$$

Theorem 3.1. *Suppose that ϕ^{n+1} and ϕ^n are periodic solutions to the scheme* (3.11)*. The following energy inequality holds for any $\Delta t > 0$,*

$$E(\phi^{n+1}) \leq E(\phi^n),$$

which means the scheme (3.11) *is unconditionally energy stable.*

Proof. In (3.7), setting $\phi = \phi^{n+1}$, $\psi = \phi^n$, we get

$$\begin{aligned} E(\phi^{n+1}) - E(\phi^n) &\leq (\delta_\phi E_c(\phi^{n+1}) - \delta_\phi E_e(\phi^n), \phi^{n+1} - \phi^n) \\ &= (\mu^n, \Delta t M \Delta \mu^n) = -\Delta t M \|\nabla \mu^n\|^2 \leq 0. \end{aligned}$$

This completes the proof of the theorem. □

4. Full-Discrete Finite Difference Scheme

Suppose $\Omega = [0, L_x] \times [0, Ly] \in R^2$. Denote the partition as $x_i = i\Delta x$, $i = 0, 1, \cdots, m$ with $\Delta x = L_x/m$ and $y_j = j\Delta y$, $j = 0, 1, \cdots, n$ with $\Delta y = L_y/n$. Define the function spaces

$$\mathcal{C}_{m\times n} = \Big\{\phi_{i,j} \in \mathbf{R}, i = 1, 2, \cdots, m,\ j = 1, 2, \cdots, n\Big\},$$

$$\mathcal{C}_{\overline{m}\times\overline{n}} = \Big\{\phi_{i,j} \in \mathbf{R}, i = 0, 1, \cdots, m,\ j = 0, 1, \cdots, n\Big\}.$$

The discrete inner product is defined as

$$(\phi, \psi) = \sum_{i=1}^{m}\sum_{j=1}^{n} \phi_{i,j}\psi_{i,j}\Delta x\Delta y, \quad \phi, \psi \in \mathcal{C}_{\overline{m}\times\overline{n}}, .$$

The discrete first order difference operators are defined as

$$d_x f_{i,j} = \frac{f_{i+\frac{1}{2},j} - f_{i-\frac{1}{2},j}}{\Delta x}, \qquad d_y f_{i,j} = \frac{f_{i,j+\frac{1}{2}} - f_{i,j-\frac{1}{2}}}{\Delta y},$$
$$D_x \phi_{i+\frac{1}{2},j} = \frac{\phi_{i+1,j} - \phi_{i,j}}{\Delta x}, \qquad D_y \phi_{i,j+\frac{1}{2}} = \frac{\phi_{i,j+1} - \phi_{i,j}}{\Delta y}.$$

Some discrete norms for $\phi \in \mathcal{C}_{\overline{m}\times\overline{n}}$ are defined as $\|\phi\|^2 = (\phi, \phi)$,

$$\|\nabla_h\phi\|^2 = \sum_{i=0}^{m-1}\sum_{j=0}^{n-1}(D_x\phi_{i+\frac{1}{2},j})^2\Delta x\Delta y + \sum_{i=0}^{m-1}\sum_{j=0}^{n-1}(D_y\phi_{i,j+\frac{1}{2}})^2\Delta x\Delta y.$$

The standard 2D Laplacian operator Δ_h is defined as

$$\Delta_h\phi_{i,j} = \frac{\phi_{i+1,j} - 2\phi_{i,j} + \phi_{i-1,j}}{\Delta x^2} + \frac{\phi_{i,j+1} - 2\phi_{i,j} + \phi_{i,j-1}}{\Delta y^2}.$$

Define the discrete energy as

$$E_h(\phi) = \sum_{i=1}^{m}\sum_{j=1}^{n} F(\phi_{i,j})\Delta x\Delta y + k_B T\kappa\|\nabla_h\phi\|^2\,. \tag{4.1}$$

and the convex splitting parts

$$\begin{aligned} E_{h,c}(\phi) =& \sum_{i=1}^{m}\sum_{j=1}^{n} k_B T\bigg(\frac{\phi_{ij}}{\tau}\ln(\frac{\alpha\phi_{ij}}{\tau}) + \frac{\phi_{ij}}{N}\ln(\frac{\beta\phi_{ij}}{\tau}) + (1-\rho\phi_{ij})\ln(1-\rho\phi_{ij}) \\ &+ \kappa|\nabla_h\phi_{ij}|^2\bigg)\Delta x\Delta y, \\ E_{h,e}(\phi) =& \sum_{i=1}^{m}\sum_{j=1}^{n} -k_B T\chi\rho\phi_{ij}(1-\rho\phi_{ij})\Delta x\Delta y\,. \end{aligned}$$

We propose the full-discrete finite difference scheme for the MMC-TDGL model (2.3) as:

$$\frac{\phi_{ij}^{n+1} - \phi_{ij}^{n}}{\Delta t} = M\Delta_h\mu_{ij}^{n}, \tag{4.2}$$

where the numerical chemical potential as

$$\mu_{ij}^n = k_B T \left(\frac{1}{\tau} \ln \frac{\alpha \phi_{ij}^{n+1}}{\tau} + \frac{1}{N} \ln \frac{\beta \phi_{ij}^{n+1}}{\tau} - \rho \ln(1 - \rho \phi_{ij}^{n+1}) - 2\kappa \Delta_h \phi_{ij}^{n+1} \right) - 2 k_B T \chi \rho^2 \phi_{ij}^n.$$

Theorem 4.1. *The discrete scheme* (4.2) *is mass conservation in discrete sense.*

Proof. Summing both sides in (4.2) for $i = 1, 2, \cdots, m,\ j = 1, 2, \cdots, n$, we get the mass conservation as below

$$\begin{aligned} &(\phi^{n+1} - \phi^n, 1) = \Delta t (M \Delta_h \mu_h^n, 1) \\ =& - \Delta t M (\nabla_h \mu_h^n, \nabla_h 1) = 0. \end{aligned}$$

This proves the theorem. □

Theorem 4.2. *The full-discrete scheme* (4.2) *is uniquely solvable for any time step size* $\Delta t > 0$.

Proof. Define the vector space

$$H := \{\phi \in \mathcal{C}_{m \times n} | (\phi, \mathbf{1}) = 0\},$$

and the inner product over H

$$(\phi_1, \phi_2)_{H,L} := (\nabla_h \psi_1, \nabla_h \psi_2) \tag{4.3}$$

where $\psi_i \in \mathcal{C}_{\overline{m} \times \overline{n}}$ is the unique solution to

$$L(\psi_i) = -\Delta_h \psi_i = \phi_i, \quad \psi_i \text{ periodic}, \quad (\psi_i, \mathbf{1}) = 0.$$

It is easily to find that

$$(\phi_1, \phi_2)_{H,L} = (\phi_1, L^{-1}(\phi_2)) = (L^{-1}(\phi_1), \phi_2)\,.$$

Without loss of generality, we suppose $\phi^n \in H$. By the mass conservation, the solution to the system (3.11) must be in H. Consider the following functional

$$G(\phi) = \frac{1}{2}(\phi, \phi)_{H,L} - (\phi, \phi^n)_{H,L} + M E_{h,c}(\phi) - (\phi, M \delta_\phi E_{h,e}(\phi^n)). \tag{4.4}$$

By the property of the bilinear form $(\cdot, \cdot)_{H,L}$, the functional above can be written as

$$G(\phi) = \frac{1}{2}(L^{-1}(\phi), \phi) - (L^{-1}(\phi), \phi^n) + M E_{h,c}(\phi) - (\phi, M \delta_\phi E_{h,e}(\phi^n)). \tag{4.5}$$

It is obviously that the functional (4.5) is strictly convex with respect to $\phi \in H$. The unique minimizer $\phi^{n+1} \in H$ of G is equivalent to solve the following system

$$\delta_\phi G(\phi^{n+1}) = L^{-1}(\phi^{n+1} - \phi^n) + M \delta_\phi E_{h,c}(\phi^{n+1}) - M \delta_\phi E_{h,e}(\phi^n) - C = 0, \tag{4.6}$$

where C is a constant. Since $L^{-1}(\phi^{n+1} - \phi^n)$ has zero mean, it must holds that $M \delta_\phi E_{h,c}(\phi^{n+1}) - M \delta_\phi E_{h,e}(\phi^n) - C$ has zero mean, which reads

$$C = \frac{1}{m \cdot n} \left(M \delta_\phi E_{h,c}(\phi^{n+1}) - M \delta_\phi E_{h,e}(\phi^n), \mathbf{1} \right).$$

Applying the operator L to both sides of (4.6), we get

$$\phi^{n+1} - \phi^n = M\Delta_h \mu_h^n + L(C).$$

Obviously, $L(C) = 0$. The uniqueness and solvability of the system (3.11) is equivalent to minimizing the convex functional G in (4.4). □

Theorem 4.3. *The full-discrete scheme* (4.2) *is unconditionally stable, which means that for any time step* $\Delta t > 0$*, it holds that*

$$E_h(\phi^{n+1}) \leq E_h(\phi^n).$$

Proof. The detailed proof of theorem (3.1) can be directly extended to the fully discrete case (4.2). Finally the following inequality holds

$$E_h(\phi^{n+1}) - E_h(\phi^n) \leq -\Delta t M \|\mu_h^n\|^2 \leq 0\,.$$ □

5. Numerical Experiments

In this section, we will present some numerical experiments. The scheme (4.2) leads to a nonlinear system of the form $NL(\phi_h^{n+1}) = 0$. We use the Newton iterative method to solve it. The initial guess for the Newton iteration at each time level is taken as the numerical solution at the previous time level. In each Newton iterative step, we need to solve a linearized system in the form

$$NL'(\phi_h^{n,\nu})\phi_h^{n+1,\nu+1} = NL'(\phi_h^{n,\nu})\phi_h^{n+1,\nu} - NL(\phi_h^{n+1,\nu}),$$

where NL' denotes the Jacobian matrix of NL. This linearized system involved in the Newton iteration is solved using conjugate gradient method. The tolerances for the conjugate gradient method and Newton iterative method are both set to be 10^{-6}.

Example 5.1. The parameters in the model (2.4) are taken as $M = 0.2$, $\chi = 0.4$, $\tau = 10^7$, $N = 800$ and $\rho = 1.0$ as in [26]. In this example, we set the temperature parameter as $T = 1$, and the initial values ϕ are random numbers around 0.65.

In our computation, we set the mesh as $m = n = 64$. The time step is taken as a constant $\Delta t = 0.001$. In Fig. 5.1, we present the phase solution contours at some selected time levels. The phase separation can be observed obviously. At the early stage the hydrogel quickly forms ordered structures from the disordered random data, then it develops slowly until it reaches the steady state, which is agree with the published results in [26].

Example 5.2. We change the initial state ϕ as random numbers around 0.35. The parameters are taken as the same as the previous ones in Example 5.1.

We show the phase solutions in Fig. 5.2. The similar phenomena is observed as in Fig. 5.1. Initially, the phase has a disordered distribution, then it quickly becomes to an ordered state until it gradually tends to a steady state with regular structure.

Example 5.3. In this example we test the effect caused by parameter temperature T. To do so, we set $T = 20$ and $T = 50$ respectively. The other parameters are taken the same settings as before. The initial values ϕ are the same as initial values given in Example 5.1.

We observed that variable T may cause the similar development of the solution, and they end with the same steady state (ignore the periodic effect) as shown in Fig. 5.3.

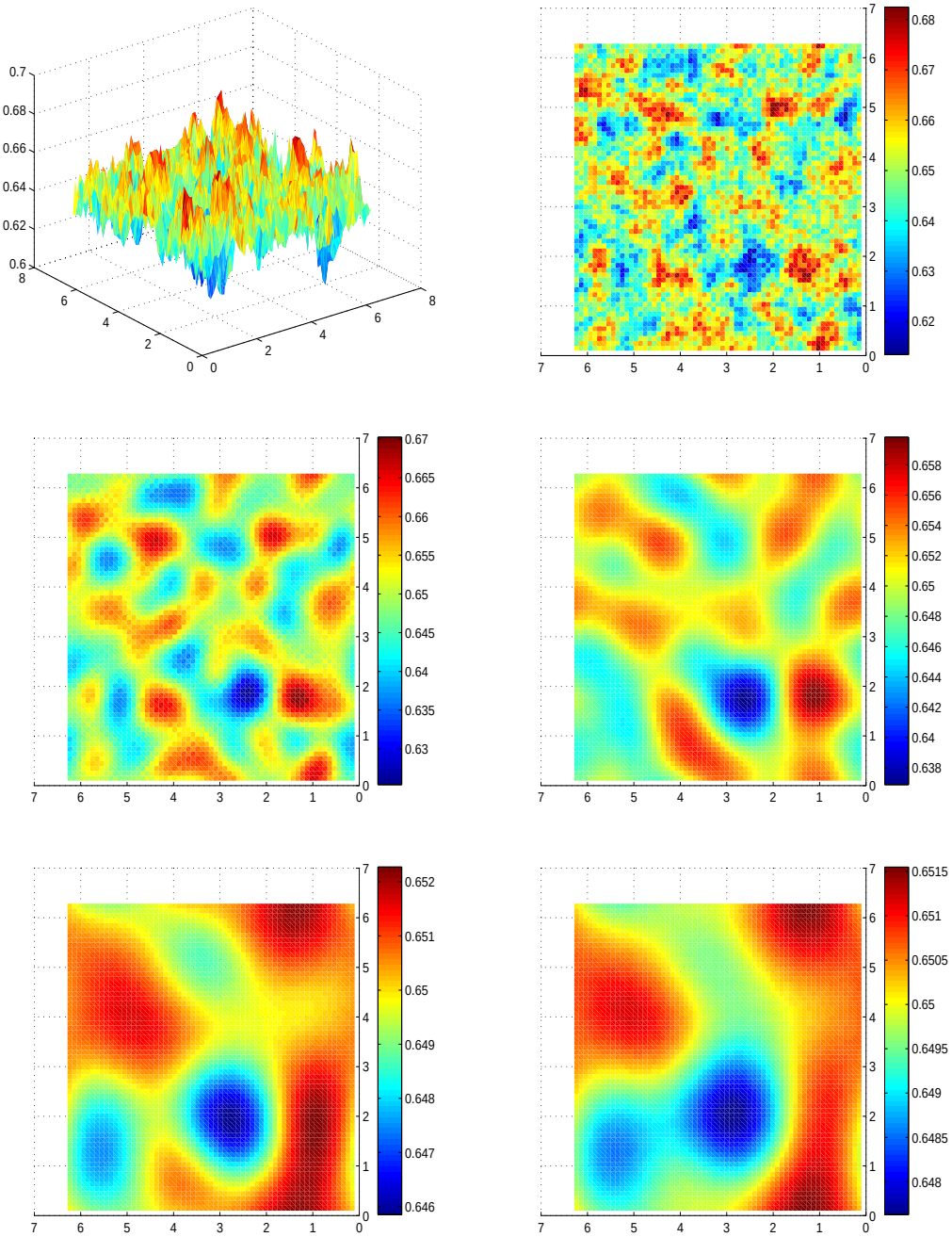

Fig. 5.1. Example 5.1: Phase solution contours at $t = 0.1, 10, 50, 100, 500, 1000$. Initial values ϕ are random numbers around 0.65.

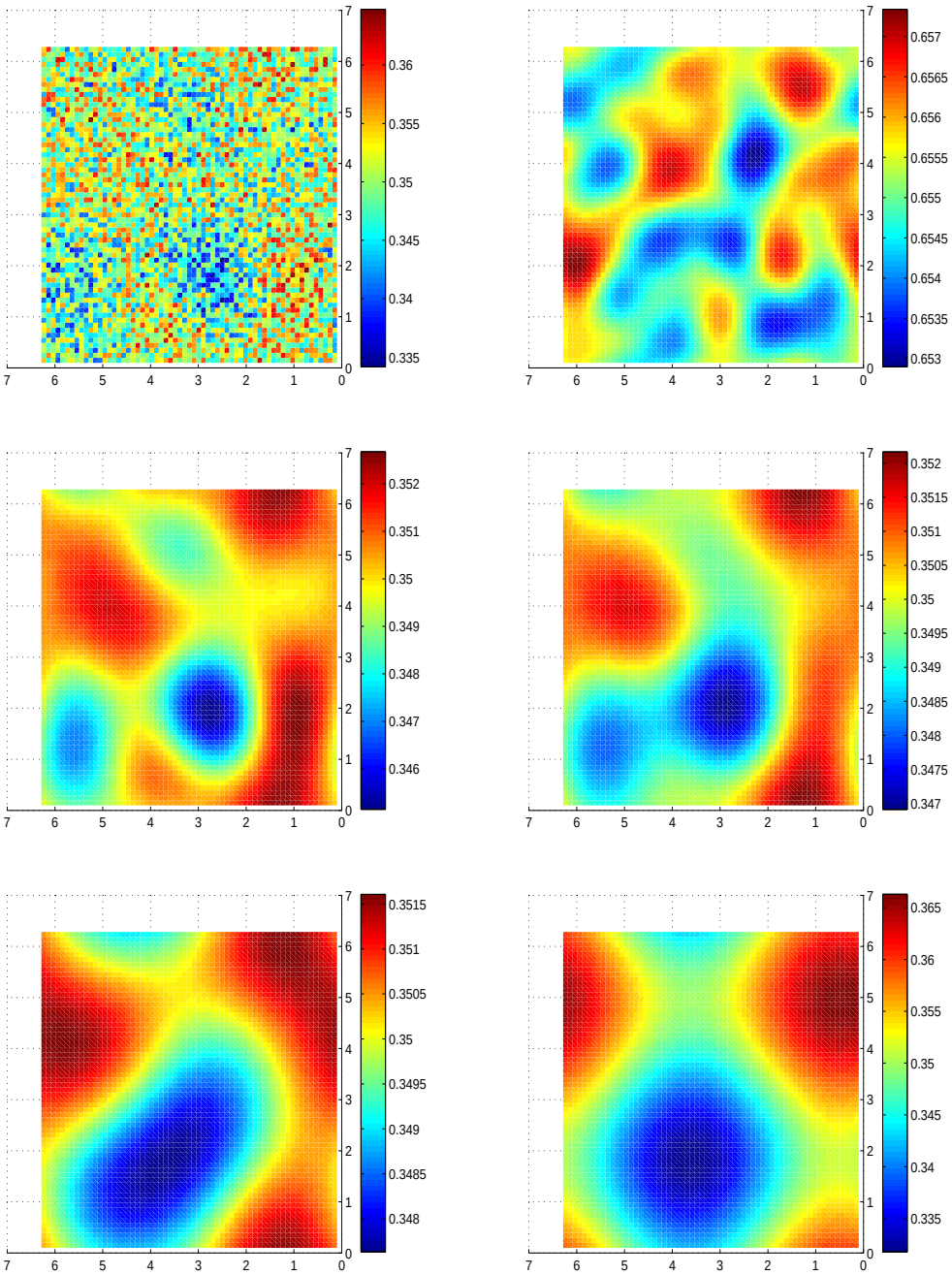

Fig. 5.2. Example 5.2: Phase solution contours at $t = 0.1, 10, 100, 500, 1000, 2000$. Initial values ϕ are random numbers around 0.35.

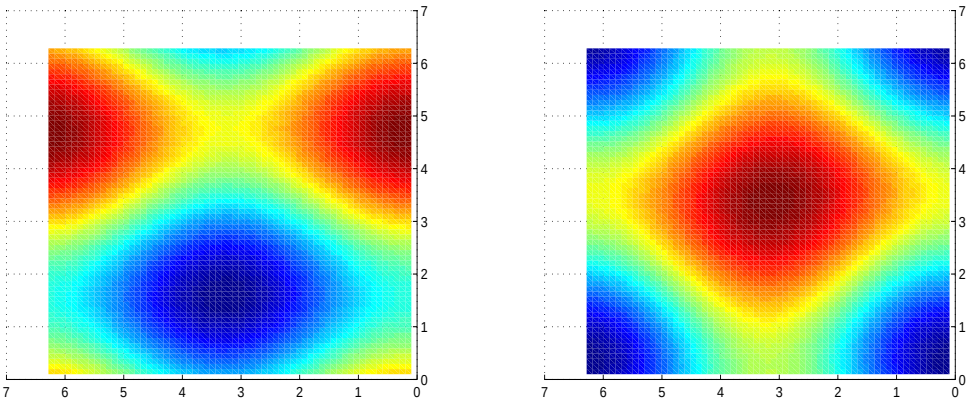

Fig. 5.3. Example 5.3: Phase solution contours at $t = 1000$, $T = 20$(left), $T = 50$(right).

6. An Adaptive Time Stepping Strategy

In the computation, it is observed that the total free energy has a quick decrement in initial stage and has a slow decay in later time, which implies the solution varies quickly in early stage and then varies slowly with respect to time variable. Hence, it is necessary to apply an adaptive time step strategy to the scheme (4.2), which can improve computational efficiency while keeping the property of energy law like the numerical experiments reported in [3].

In Section 4, we have proved that the nonlinear scheme (4.2) is unconditionally energy stable, which allows to employ large time step during numerical simulations [17–19]. For the sake of accuracy, a very large time step is unacceptable except in the time intervals where solutions change considerably little. In the following simulations, we will conduct numerical simulations under different constant time steps, such as $\Delta t = 0.001$, $\Delta t = 0.005$, $\Delta t = 0.01$ and $\Delta t = 0.05$. Here, the initial values are taken as same as the ones given in Example **??**. In order to test the numerical accuracy with respect to time variable, we take the numerical solution obtained using $\Delta t = 10^{-4}$, $m = n = 512$ as 'exact' solution. We define the error in L^2-norm as

$$\|e_h(t)\| = \sqrt{\sum_{i=1}^{m}\sum_{j=1}^{n}(\phi_{i,j}(t) - \phi(x_i, y_j, t))^2 \Delta x \Delta y}, \tag{6.1}$$

where $\phi(x_i, y_j, t)$ is the 'exact' solution at t. $\phi_{i,j}(t)$ is the numerical solution. We set the temperature parameter as $T = 1$. In Figs. 6.1, we present the total free energy evolution against time. It is seen that the total free energies under different constant time steps are all decreasing over time, which indicates that numerical solutions under different constant time steps are consistent with the property of energy stability analyzed in Section 4. Also, it is observed that the energies with different constant time steps tend to almost the same state though they have distinct dynamical processes. The obvious reason is that constant large time step may cause poor accuracy during the early stage where the energy has a quick change. To get more facts of the phenomena we do the same numerical experiments using different temperature. In Figs. 6.2 we set $T = 50$ and present the energy development. The similar phenomena as shown in Figs. 6.1 is observed. With larger temperature parameter, the constant

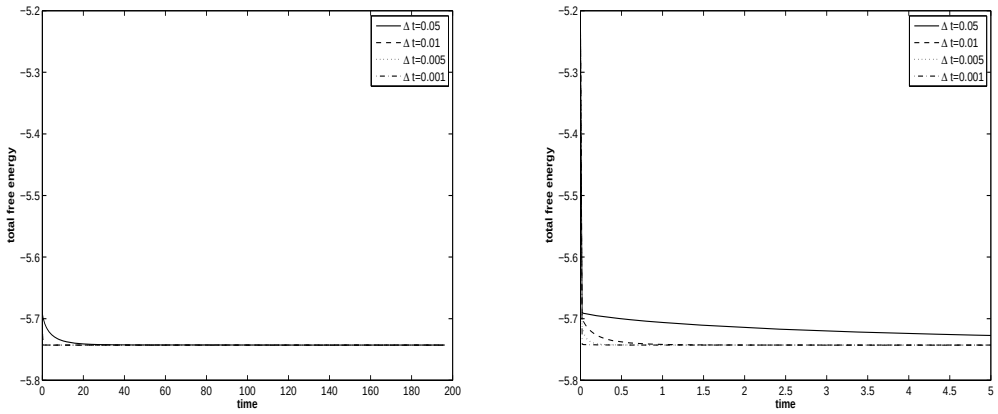

Fig. 6.1. Total energy evolution over time with $T = 1$ under different constant time steps.

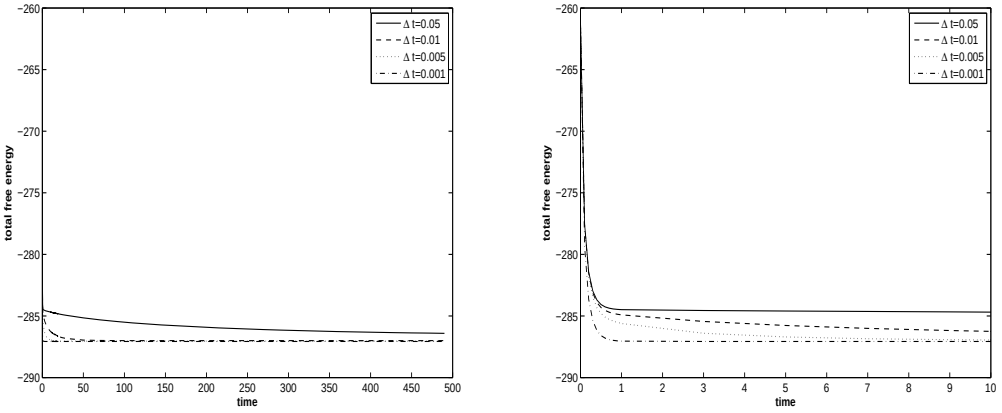

Fig. 6.2. Total energy evolution over time at $T = 50$ under different constant time step.

time step seems to cause more deviate of the energy curve from the energy curve obtained by 'exact' solution.

Motivated by the facts shown in Figs. 6.1 and 6.2, we will apply an adaptive time step strategy to the numerical scheme (4.2). We employ small time steps when the total free energy decreases significantly, which mean solutions have a large variation, and we will choose large time steps when total free energy has a slow change. Following [3], according to the choice of the adaptive time step and the definition of total free energy in this equation, we improve adaptive time step monitor:

$$\Delta t = \max(\Delta t_{\min}, \lambda(T,t)\frac{\Delta t_{\max}}{\sqrt{1+\gamma|E'(t)|^2}}). \tag{6.2}$$

Here γ is a constant parameter, $E'(t)$ is the derivative of $E(t)$ and $\lambda(T,t)$ is introduced to ensure accuracy and efficiency. If we carefully compare the energy curves shown in Figs. 6.1 and 6.2, we find that the bigger parameter T may cause more significant variation on the energy curve. By rough estimate, for the same increment of E, the derivative $|E'(t)|^2$ with $T = 50$ is 2500 times larger than the derivative of it with $T = 1$. So we hope to involve T in the monitor

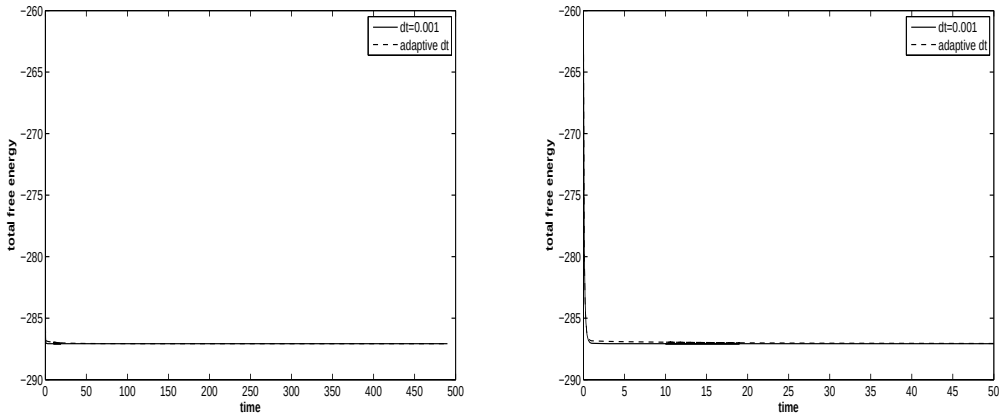

Fig. 6.3. Total free energy evolution development comparison.

defined in (6.2) to make it also dependent on T besides the energy derivative. In the following simulation, we choose $\Delta t_{\min} = 0.001, \Delta t_{\max} = 0.1, \gamma = 1000$. The multiplier $\lambda(T,t)$ is designed as:

$$\lambda(T,t) = \begin{cases} 1 & \text{if} \quad 0 \le t \le 100 \\ 1.5 & \text{if} \quad 100 < t \le 200 \\ 2 & \text{if} \quad 200 < t \le 300 \\ 3 & \text{if} \quad 300 < t \le 400 \\ 4 & \text{if} \quad 400 < t \le 500 \\ 5 & \text{if} \quad t > 500\,. \end{cases}$$

The CPU time consumed at some selected time levels using different time steps are shown in Table 6.1. It is observed that the CPU time consumed using adaptive time steps is much less

Table 6.1: CPU time costs comparison.

CPU time	$t = 1$	$t = 10$	$t = 100$	$t = 500$
constant $\Delta t = 0.05$	47.8	388.6	3416.9	14341.4
constant $\Delta t = 0.01$	149.6	905.6	4190.2	5987.2
constant $\Delta t = 0.005$	151.8	948.5	2335.1	3920.5
constant $\Delta t = 0.001$	184.5	419.7	2125.2	10485.2
adaptive Δt	110.1	202.7	668.8	2809.4

than the one using constant time steps. From Figs. 6.3, we can see that the difference of total free energy evolution is very small under constant time step $\Delta t = 0.001$ and the adaptive time step. During the initial stage, the adaptive time step produced by the monitor (6.2) is close to $\Delta t = 0.001$, so we we get a good approximation. However, as the system evolves for some time, the free energy changes little indicating that the change of ϕ is also very small. As a result, the monitor function (6.2) determines a large time step which might be 100 times bigger than 0.001, while little error is caused.

In Table 6.2 we list the comparison of the errors in L^2-norm obtained using different time steps at some selected time levels. It is easily seen that larger constant time step lead to larger errors which is consistent with the analysis given above. The L^2-error with adaptive time strategy is considerably small during the whole process of simulation, which indicates that the adaptive method is not only efficient but also accurate.

Table 6.2: Errors in L^2-norm comparison using different time steps.

L^2-error	$t=1$	$t=10$	$t=100$	$t=200$
constant $\Delta t=0.05$	0.031	0.0286	0.0256	0.0376
constant $\Delta t=0.01$	0.0267	0.0152	0.0086	0.0083
constant $\Delta t=0.005$	0.0198	0.0058	0.0037	0.0056
adaptive Δt	0.0095	0.0042	0.000987	0.000325

7. Concluding Remarks

In this paper, we proposed an unconditional energy stable finite difference scheme for the TDGL model based on convex splitting method. The unconditional energy stability is proved theoretically. The unique solvability is proved through an equivalent convex discrete functional. The numerical experiments are carried out to verify the theoretical results. In the future, we will develop a robust adaptive time step monitor function which evolves less artificial parameters. It should be dependent on more essential properties of the system. The proposed numerical method may be considered to be extended to the case with variable coefficients such as $\kappa(\phi), M(\phi), T(\phi)$.

Acknowledgments. The authors would like to thank Dr. Jun Han for his help in coding. Hui Zhang was supported by the Fundamental Research Funds for the Central Universities, NSFC-RGC No. 11261160486 the Ministry of education program for New Century Excellent Talents Project NCET-12-0053 and National NSF of China under grant 11571054, 11471046. Zhengru Zhang was partially supported by the Fundamental Research Funds for the Central Universities and National NSF of China under grant 11271048, 1130021 and 11571054.

References

[1] A. Chakrabarti, R. Toral, J. D. Gunton, et al, Dynamics of phase separation in a binary polymer blend of critical composition, *J. Chem. Phys*, **92**(1990), 6899-6909.

[2] M. Fermeglia, S. Pricl, Multiscale modeling for polymer systems of industrial interest, *Progress in Organic Coatings*, **58**(2007), 187-199.

[3] H.W. Gibson, M.C. Bheda, P.T. Engen, Rotaxanes, catenanes, polyrotaxanes,polycatenanes and related materials, *Prog. Polym. Sci.*, **19**(1994), 843-945.

[4] J.P. Gong, Y. Katsuyama, T. Kurokawa, et al, Double network hydrogels with extremely high mechanical strength, *Advanced Materials*, **15**(2003), 1155-1158.

[5] W.W. Graessley, D.S. Pearson, Stress-strain behavior in polymer networks containing nonlocalized junctions, *J. Chem. Phys.*, **66**(1977), 3363-3370.

[6] S.T. Gu, H. Zhang and Z.R. Zhang, An energy-stable finite-difference scheme for the binary fluid-surfactant system, *J. Comput. Phys.*, **270**(2014), 416-431.

[7] M. Huang, H. Furukawa, Y. Tanaka, et al, Importance of entanglements between first and second components in high-strength double network gels, *Macromolecules*, **40**(2007), 6658-6664.

[8] K. Harag, T. Takehisa, Nanocomposite hydrogels: a unique organic-inorganic network structure with extraordinary mechanical, optical, and swelling/deswelling properties. *Advanced Materials*, **14**(2002), 1120-1124.

[9] T. Huang, H.G. Xu, K.X. Jiao, et al, A novel hydrogel with high mechanical strength: A macromolecular microsphere composite hydrogel, *Advanced Materials*, **19**(2007), 1622-1626.

[10] J.A. Johnson, N.J. Turro, J.T. Koberstein, et al, Some hydrogel having novel molecular structure, *Progress in Polymer Science*, **35**(2010), 332-337.

[11] S.S. Jang, M. Yashaar, S. Kalani, et al, Mechanical and transport properties of the poly(ethylene oxide)-poly(acrylic acid) double network hydrogel from molecular dynamic simulations, *J. Phys. Chem. B*, **111**(2007), 1729-1737.

[12] S.S. Jang, M. Yashaar, S. Kalani, et al, Corrections to mechanical and transport properties of the poly(ethylene oxide)-poly(acrylic acid) double network hydrogel from molecular dynamic simulations, *J. Phys. Chem. B*, **111** (2007), 14440/1.

[13] K. Luo, The morphology and dynamics of polymerization of polymerization-induced phase separation, *Euro. Poly. J.*, **42**(2006), 1499-1505.

[14] D. Nwabunma, H.W. Chiu, T. Kyu; Theoretical investigation on dynamics of photopoly merization-induced phase separation and morphology development in nematic liquid crystal/polymer mixtures, *J. Chem. Phys.*, **113**(2000), 6429-6436.

[15] Y. Okumura, K. Ito, The polyrotaxane gel: a topological gel by figure-of-eight cross-links, *Advanced Materials*, **13**(2001), 485-487.

[16] A. Okada, A. Usuki, Twenty years of polymer-clay nanocomposites, *Macromol. Mater. Eng.*, **291**(2006), 1449-1476.

[17] Z.H. Qiao, Z.R. Zhang, T. Tang, An adaptive time-stepping strategy for the molecular beam epitaxy models, *SIAM J. Sci. Comput.*, **33**(2011), 1395-1414.

[18] G. Soderlind, Automatic control and adaptive time-stepping, *Numer. Algorighms*, **31**(2002), 281-310.

[19] G. Soderlind, L. Wang, Adaptive time-stepping and computational stability, *J. Comput. Appl. Math.*, **185**(2006), 225-243.

[20] Z.J. Tan, Z.R. Zhang, Y.Q. Huang et al, Moving mesh methods with locally varying time steps, *J. Comput. Phys.*, **200**(2004), 347-367.

[21] S.M. Wise, C. Wang, J.S. Lowengrub, An energy-stable and convergent finite-difference scheme for the phase field crystal equation, *SIAM J. Numer. Anal.*, **47**(2009), 2269-2288.

[22] X.C. Xiao, L.Y. Chu, W.M. Chen, et al, Monodispersed thermosponsive hydrogel micropsheres with a volume phase transition driven by hydrogen boning, *Ploymer*, **46**(2005), 3199-3209.

[23] X.M. Yao, H. Zhang, Kinetic model for the large deformation of cylindrical gels, *J. Theoret. Comput. Chem*, **13**(2014), 1450032.

[24] C.H. Yuan, H. Zhang, Self-consistent mean field model of hydrogel and its numerical simulation, *J. Theoret. Comput. Chem*, **12**(2013), 1350048.

[25] Q.H. Zeng, A.B. Yu, G.Q. LU, Multiscale modeling and simulation of polymer nanocomposite, *Progress in Polymer Science*, **33**(2008), 199-269.

[26] D. Zhai, H. Zhang, Investigation on the application of the TDGL equation in macromolecular microsphere composite hydrogel, *Soft Matter*, **9**(2013), 820-825.